EXCLI Journal 2026;25:290-309 – ISSN 1611-2156
Received: November 03, 2025, accepted: January 14, 2026, published: January 23, 2026

Original article:

LONG-TERM WESTERN DIET FEEDING IMPAIRS HEPATIC VITAMIN D METABOLISM AND PROMOTES BONE LOSS IN MICE

Pengcheng Zhou[1,#], Mohammad Majd Hammour[1,#], Romina H. Aspera-Werz[1], Sabrina Ehnert[1], Maiju Myllys[2], Zaynab Hobloss[2], Reham Hassan[2,3], Daniela González[2], Rama Hendawi[2,4], Karolina Edlund[2], Sandra Hans[5], Matthias W. Laschke[5], Ahmed Ghallab[2,3], Jan G. Hengstler[2,†], Andreas K. Nüssler[1,†,*], Tanja C. Maisenbacher[1,†]

[1] Siegfried Weller Institute for Trauma Research, Department of Trauma and Reconstructive Surgery, Eberhard-Karls-University Tuebingen, BG Unfallklinik, 72076 Tuebingen, Germany
[2] Leibniz Research Centre for Working Environment and Human Factors (IfADo), 44139 Dortmund, Germany
[3] Forensic Medicine and Toxicology Department, Faculty of Veterinary Medicine, Qena University, Qena, Egypt
[4] Department of Biomedical Sciences, Faculty of Medicine and Health Sciences, An-Najah National University, PO Box 7, Nablus, Palestine
[5] Institute for Clinical and Experimental Surgery, Saarland University, PharmaScienceHub (PSH), 66421 Homburg, Germany

[#,†] These authors have contributed equally as first authors ([#]) and last authors ([†]).

[*] **Corresponding author:** Andreas Nüssler, Siegfried Weller Institute for Trauma Research, Department of Trauma and Reconstructive Surgery, Eberhard-Karls-University Tuebingen, BG Unfallklinik, 72076 Tuebingen, Germany. E-mail: Andreas.nuessler@gmail.com

https://dx.doi.org/10.17179/excli2025-9085

ABSTRACT

Obesity and metabolic dysfunction-associated fatty liver disease (MAFLD) are increasingly recognized as risk factors for skeletal fragility, yet the mechanisms linking these conditions to impaired bone health remain poorly defined. The liver is central to vitamin D homeostasis through 25-hydroxylation, while skeletal responsiveness relies on vitamin D receptor (VDR) signaling. Disruption of either process may compromise bone remodeling. In this study, we investigated the long-term effects of Western diet (WD) feeding on hepatic vitamin D metabolism and bone integrity in a mouse model. Male C57BL/6N mice were fed a standard diet (SD) or WD for 48 weeks. WD-fed mice developed obesity, hepatic injury, and trabecular bone deterioration characterized by reduced bone mineral density and increased trabecular separation. Although trabecular architecture was compromised, three-point bending revealed no significant impairment in cortical bone mechanical properties. Histological analyses showed increased bone marrow adiposity and macrophage/monocyte lineage cells. Bone gene expression profiling indicated enhanced osteoclastogenic signaling. Hepatic transcriptomics demonstrated marked downregulation of key 25-hydroxylases (*Cyp2r1*, *Cyp27a1*) and vitamin D–binding protein, accompanied by reduced circulating 25-hydroxyvitamin D. Bone tissue also exhibited decreased VDR protein abundance. Together, these findings suggest that long-term WD-induced obesity and hepatic dysfunction impair hepatic vitamin D metabolism and diminish skeletal vitamin D responsiveness, contributing to bone fragility. Targeting the liver–bone axis and restoring vitamin D homeostasis may provide therapeutic potential for obesity-related bone loss.

EXCLI Journal 2026;25:290-309 – ISSN 1611-2156
Received: November 03, 2025, accepted: January 14, 2026, published: January 23, 2026

Keywords: Bone loss, osteoporosis, liver-bone axis, MAFLD, Vitamin D, Vitamin D receptor

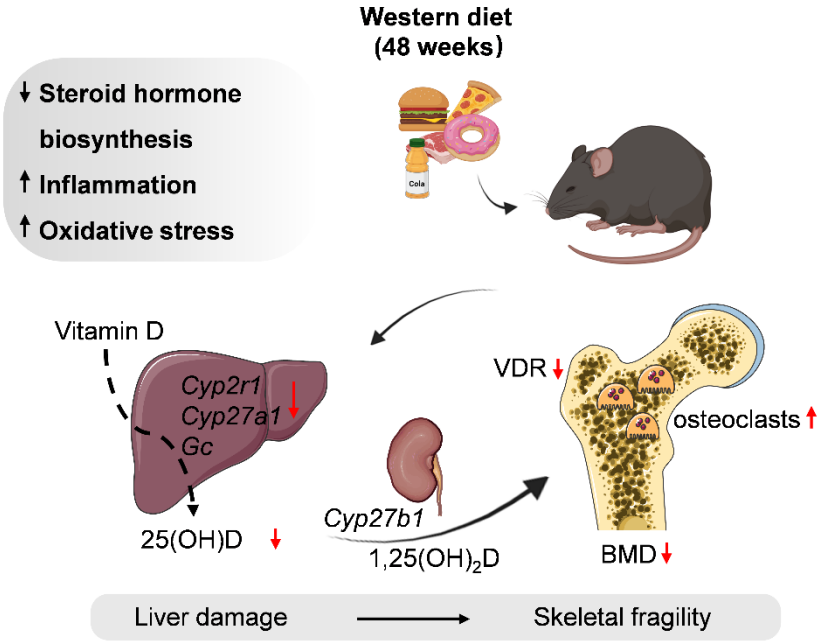

Figure 1: Graphical abstract

INTRODUCTION

Obesity has emerged as a global crisis, with projections indicating that more than 1 billion individuals will be living with the condition by 2030 (Bathina and Armamento-Villareal, 2023). As a complex metabolic disorder, obesity is intricately associated with a wide range of comorbidities, including type 2 diabetes, metabolic dysfunction-associated fatty liver disease (MAFLD), lower circulating 25-hydroxyvitamin D (25(OH)D), and disrupted bone homeostasis (Kawai et al., 2021). Paradoxically, despite higher body weight and increased mechanical loading, obese individuals are at greater risk for fractures (Compston et al., 2011; Prieto-Alhambra et al., 2012; Gkastaris et al., 2020), suggesting that factors beyond body weight influence skeletal integrity. Clinical and experimental evidence increasingly points to a complex interplay between MAFLD, obesity, and bone fragility (Zhao et al., 2023; Gao et al., 2024). However, the mechanisms underlying the elevated fracture risk associated with obesity remain unknown.

Vitamin D, a steroid hormone synthesized in the skin *via* UVB-induced conversion or obtained from dietary sources, plays a crucial role in regulating calcium-phosphate homeostasis and maintaining skeletal integrity (Akter et al., 2022). The liver plays a central role in vitamin D metabolism by catalyzing the first hydroxylation step, converting vitamin D into 25(OH)D (Wintermeyer et al., 2016), the major circulating form and substrate for renal 1α-hydroxylation to generate the active metabolite 1,25-dihydroxyvitamin D (1,25(OH)$_2$D). This active form regulates calcium-phosphate homeostasis and bone remodeling (Wintermeyer et al., 2016; Ehnert et al., 2019). Clinically, 25(OH)D is the most commonly used biomarker of vitamin D status. However, renal 1α-hydroxylation is tightly regulated by phosphate, parathyroid hormone (PTH), and fibroblast growth factor-23 (FGF23), and therefore does not necessarily correlate with 25(OH)D across physiological or disease states (Jacquillet and Unwin, 2019; Latic and Erben, 2021). Therefore, inferences about functional vitamin D sufficiency from 25(OH)D

alone must be made with caution (Serdar et al., 2024). Nevertheless, lower 25(OH)D levels are frequently observed in obesity, with a substantial proportion of individuals falling below 30 ng/mL (Via, 2012; Turer et al., 2013). Observational studies suggest that every 10 ng/mL increase in serum 25(OH)D concentration is associated with a 7 % reduction in the risk of any fracture and a 20 % reduction in the risk of hip fracture (Yao et al., 2019). Several mechanisms have been proposed to explain this consistent reduction in circulating 25(OH)D, including the sequestration of vitamin D by excess body fat, reduced sun exposure, chronic inflammation, and gut microbiota dysbiosis (Bennour et al., 2022). However, the evidence remains limited and inconclusive.

Beyond vitamin D metabolism, MAFLD-related hepatic dysfunction may influence bone health through additional mechanisms, including chronic inflammation, altered lipid handling, and impaired bile acid synthesis, which contributes to dietary vitamin D absorption. These processes, combined with systemic metabolic stress, may disrupt bone remodeling and favor resorption. Despite these associations, the mechanistic link between long-term WD-induced hepatic injury and bone remodeling remains poorly understood. Most preclinical studies employ short-term dietary interventions, which fail to capture chronic metabolic adaptations relevant to human disease. To address these gaps, we established a 48-week high-fat, high-carbohydrate WD model that induces obesity and MAFLD-like hepatic injury. The WD model has been comprehensively characterized in a previous study by Ghallab et al. (2021), who identified a sequence of pathological events during MAFLD progression in the same cohort of mice, closely mirroring the progression of human disease. Building on this established dataset not only ensures translational relevance but also adheres to the principles of the 3Rs by reducing the need for additional animal cohorts.

In this study, we investigated the hepatic vitamin D 25-hydroxylases, vitamin D-binding protein (DBP) expression, circulating concentrations of 25(OH)D, skeletal VDR abundance and associated bone alterations. Our objective is to elucidate how hepatic dysfunction contributes to disordered vitamin D metabolism and skeletal fragility in individuals with obesity and MAFLD, thereby highlighting potential therapeutic targets for the clinical management of obesity-related osteoporosis.

MATERIALS AND METHODS

Animals

24 male, 8 weeks old C57BL/6N mice were obtained from Janvier Labs, Le Genest-Saint-Isle, France. Mice were randomly assigned to either the SD or WD group using a random number generator. 12 were fed a SD (Ssniff R/M-H, 10 mm Standard diet (Ssniff, Soest, Germany)), 12 were fed a high-carbohydrate, high-fat and high-cholesterol WD (Research diets, Inc., #D16022301, New Brunswick, NJ, USA) (Ghallab et al., 2021). Table 1 summarizes the nutrient composition per 100 g as provided by the manufacturer. The mice were housed individually with free access to food and water, 25 °C temperature, and under 12 h light/dark cycles. They were weighed weekly and sacrificed at week 48. The *femora* and *tibiae* were harvested, soft tissue was removed, the bones were weighed and measured, and were individually frozen in Eppendorf tubes at -80 °C. All experiments were approved by the local governmental animal welfare committee (LANUV, North Rhine-Westphalia, Germany; application number: 81-02.04. 2020.A304).

EXCLI Journal 2026;25:290-309 – ISSN 1611-2156
Received: November 03, 2025, accepted: January 14, 2026, published: January 23, 2026

Table 1: Nutrient composition of the standard diet and Western diet per 100 g

Nutrient		Standard Diet (SD)	Western Diet (WD)
Energy [kcal]		322	450
Total Protein [g]		19	22
Amino Acids [g]	Ala	0.82	0.56
	Arg	1.19	0.65
	Asn	0	0.77
	Asp	1.79	0.56
	Cys	0.35	0.47
	Gln	0	1.89
	Glu	4.1	2.29
	Gly	0.88	0.33
	His	0.48	0.5
	Ile	0.79	0.83
	Leu	1.39	1.73
	Lys	1	1.44
	Met	0.33	0.56
	Phe	0.88	0.92
	Pro	1.29	1.94
	Ser	0.99	1.1
	Thr	0.71	0.79
	Trp	0.25	0.23
	Tyr	0.61	1
	Val	0.90	1.02
Fat [g]	Total	3.3	20
	Content	Crude Fat 3.3	Soybean Oil 2.77 Peimex-Z, Non-Trans Fat 14.9 Lard 2.21
Fatty Acids [g]	Saturated	C14, Myristic 0.01 C16, Palmitic 0.45 C18, Stearic 0.09 C20, Arachidic 0.01	C12, Lauric 0.06 C14, Myristic 0.19 C16, Palmitic 7.01 C17 0.01 C18, Stearic 1.4 C20, Arachidic 0.07 C22, Behenic 0.01
	Monounsaturated	C16:1, Palmitoleic, 0.01 C18:1, Oleic 0.62	C16:1 Palmitoleic, 0.03 C18:1, Oleic 7.01 C20:1, Eicosenoic 0.02
	Polyunsaturated	C18:2, Linoleic 1.76 C18:3, Linolenic 0.23	C18:2, Linoleic 3.46 C18:3, Linolenic 0.28 C20:2, Eicosadienoic 0.02 C20:4, Arachidonic 0.01
	Trans fats	-	C18:1, Elaidic 0.06 C18:2, Trans 0.03 C18:3, Trans 0.01
Carbohydrate [g]	Total	41.3	45
	Content	Starch 35.9 Sugar 5.4	Maltodextrin 10 11.1 Fructose 22.1 Sucrose 10.6
Mineral [mg]	Ca	1000	670
	P	700	330
	K	920	660
	S	0	37
	Mg	220	55
	Na	240	111
	Cl	0	177

	Cu	1.5	0.664
	I	0.21	0.022
	Fe	18.9	4.98
	Mn	6.8	6.53
	Se	0.03	0.018
	Zn	9.1	3.21
	Cr	0	0.221
	F	0	0.1
	Mo	0	0.177
Vitamins [mg]	Vit A	450	132.74
	Vit B1	1.8	0.664
	Vit B2	2.2	0.664
	Vit B6	2.1	0.774
	Vit B12	0.01	0.011
	Vit D3	2.75	2.77
	Vit E	11	3.71
	Menadione	0.7	0.055
	Biotin	0.051	0.022
	Folic Acid	0.7	0.221
	Niacin	11.5	3.318
	Panthenic Acid	4	1.77
	Choline	137	88.4
Cholesterol [g]		0	1.99

Plasma biochemical and metabolite analysis

Alanine aminotransferase (ALT), aspartate aminotransferase (AST), and alkaline phosphatase (ALP) were quantified in freshly collected heparinized cardiac blood using a Piccolo Xpress Chemistry Analyzer (Abaxis/Hitado) together with the Piccolo General Chemistry 13 Panel Kit (Hitado, AB-114-400-0029). Plasma concentration of 25(OH)D was determined using commercial ELISA kit (Immunodiagnostic Systems, AC-57SF1) following the manufacturers' instructions. Absorbance was recorded at 450 nm using an Omega plate reader, and analyte concentrations were calculated based on standard curves generated from known 25(OH)D standards.

µCT analysis

The right *femora* were stored in Eppendorf tubes and scanned using a Skyscan (1172, Bruker, Billerica, MA USA) at a spatial resolution of 9 µm. A standardized scanning setup was used: tube voltage: 50 kV, exposure time: 1150 ms, current: 500 µA, rotation steps: 0.30 °, filter: 0.5 mm aluminum. Images were reconstructed using nRecon (Bruker, Billerica, MA, US). For analysis, CTAnalyser (Bruker, Billerica, MA, USA) was used. For calibration of gray values phantom rods (calcium hydroxyapatite (CaHA)) with known bone mineral density values (0.250 g and 0.750 g (CaHA/cm^3)) were used. The distal femoral growth plate was identified as reference. The region of interest (ROI) for cancellous bone analysis was starting 0.45 mm (50 slices) proximal to the reference and extending 0.54 mm (60 slices). The ROIs were contoured manually and interpolated between each transversal slide. The tissue volume (TV, (µm^3)), bone volume (BV, (µm^3)), the bone volume fraction of the tissue volume (BV/TV), the trabecular number (Tb. N (1/µm)), the trabecular separation (Tb. Sp (µm)) and the trabecular thickness (Tb. Th (µm)) from trabecular ROIs were determined individually.

Biomechanical analysis

The right *tibiae* were brought to room temperature. Biomechanical testing was performed by a three-point bending device (Zwick/Roell Z2.5, ZwickRoell GmbH & Co. KG, Ulm, Germany). For standardized measuring conditions, all *tibiae* were placed on the ventral side downwards with a 10 mm distance between the supports. The measurement was carried out with a constant speed of 0.15 mm/s, orthogonal to the axis of the tibiae. Loading was automatically stopped when the bones got fractured.

Histomorphometry

Following µCT scanning, the right *femora* were subjected to histological analysis. The bones were initially fixed in IHC zinc fixative (BD Pharmingen, San Diego, CA) for 24 h. Subsequently, they were decalcified in 13 % EDTA solution for two weeks and then embedded in paraffin. Longitudinal sections, 5 µm thick, were cut from the bones for further staining. For immunohistochemical staining, sections were incubated for 1 h with a monoclonal rabbit anti-mouse antibody against perilipin (1:200; Cell Signaling Technology, Danvers, MA, USA) and a rabbit anti-CD163 (1:300; Abcam, Cambridge, UK) as the primary antibody. After washing, the primary antibody was detected using A goat anti-rabbit peroxidase-labelled secondary antibody (1:100; Jackson ImmunoResearch Laboratories, West Grove, PA, USA).

Images were acquired using an EVOS® Digital Inverted Microscope at 40× magnification. Four to eight fields from the proximal femur were randomly selected and analyzed using QuPath (Version 0.5.1). Background correction was applied using the "estimate stain vectors" function. Positive cells were defined as nuclei surrounded by specific immunoreactive staining and detected using the "Positive Cell Detection" tool. For nuclear size quantification, images were imported into ImageJ (NIH, Bethesda, MD, USA). Eight nuclei per section were randomly selected and manually segmented using the Wand tool. Nuclear cross-sectional area was measured, and mean values were calculated for each group. This approach was chosen because cytoplasmic boundaries are indistinct in bone marrow tissue, making the nuclear area a reliable surrogate for cell size.

RNA isolation and RT-PCR analysis

The left *femora* and *tibiae* were frosted with liquid nitrogen in a pre-cooled mortar and crushed into small pieces. The pieces were transferred into a tube and covered with 500 µL of self-made Trifast (0.8 M guanidine thiocyanate, 0.4 M ammonium thiocyanate, 0.1 M sodium acetate solution, 5 % glycerol, 38 % phenol). After overnight freezing at -80°C, 100 µL of chloroform (per 500 µL of self-made Trifast) were added, thoroughly mixed and incubated for 5 min. After centrifugation at 14,000 × g for 10 min, the upper clear phase was mixed with 100 % ethanol to a final ethanol concentration of 40 %. The RNA isolation was continued with the All-In-One DNA/RNA/Protein Miniprep Kit (Bio Basic Inc., Canada) and carried out according to the manufacturer's instructions. During the isolation genomic DNA was digested with DNAse I (EN0521, Thermo Fisher, USA). RNA was quantified with the LVIS Plate on an Omega Plate Reader (BMG Labtech). RNA was transcribed into cDNA with the First Strand cDNA Synthesis Kit (Thermo Fisher) according to the manufacturer's instructions. RT-PCR was performed using 2× Red Taq Master Mix (Biozym, Oldendorf, Germany). Primer pairs were designed from NCBI GenBank sequences using Primer-BLAST, and optimized amplification conditions for each gene target are summarized in Supplementary information (Supplementary Table 1). Each biological sample was analyzed in technical duplicate, and the mean normalized gray value was used for statistical analysis. This semi-quantitative approach allowed for relative comparison of gene expression levels between experimental groups.

Western blot

The right *tibiae* were crushed into small pieces with liquid nitrogen in a pre-cooled mortar. The pieces were then transferred into microcentrifuge tubes and resuspended in 300 µL of ice-cold RIPA lysis buffer (10 mM TRIS, 100 mM NaCl, 0.5 % Tergitol NP40, 0.5 % deoxycholic acid, 10 mM EDTA, protease and phosphatase inhibitors, pH = 7.6). Samples were incubated on ice for 30 minutes to ensure complete lysis, followed by centrifugation at 13,000 × g for 10 minutes at 4 °C to remove insoluble debris. Protein concentrations in the supernatant were measured using the Lowry assay. Equal amounts of protein (40 µg per lane) were loaded on 10 % SDS-PAGE gels and electro-transferred onto nitrocellulose membranes using a standard wet-transfer system. Membranes were stained with Ponceau S to verify transfer efficiency and subsequently blocked in 5 % bovine serum albumin (BSA) dissolved in TBS-T for 1 hour at room temperature. Primary antibody incubation was performed overnight at 4 °C using antibodies against VDR (1:500, Santa Cruz Biotechnology, #13133) and HPRT (1:500, Santa Cruz Biotechnology, #376938), the latter serving as the loading control. After washing with TBS-T, membranes were incubated with horseradish peroxidase (HRP)-conjugated secondary antibodies anti-mouse lgG Kappa BP (1:5000, Santa Cruz Biotechnology, #516102) for 2 hours. Protein bands were visualized using an enhanced chemiluminescence (ECL) detection system and imaged with the INTAS Chemocam (INTAS, Göttingen, Germany).

RNA-Seq analysis and bioinformatics

Liver tissues were collected from SD and WD-fed mice (N = 5 per group). Sample preparation and RNA-Seq analysis were performed as previously described (Ghallab et al., 2021). Differential gene expression analysis was conducted using the DESeq2 package (v1.46.0) in R (v4.4.2). Genes with an absolute log2 fold change (|log2FC|) $\geqslant$ 2 and a false discovery rate (FDR)-adjusted p-value $\leqslant$ 0.001 were considered DEGs. For functional enrichment analysis, DEGs were analyzed using the GO and KEGG databases through the g:Profiler (Kolberg et al., 2023). Additionally, the Gene Set Enrichment Analysis (GSEA) was performed using the software (v4.4.0), with defined vitamin D metabolism gene set (*Cyp2r1, Cyp27a1, Cyp24a1, Gc, Lrp2, Dhcr7, Rxra, Vdr, Cyp27b1*) (Subramanian et al., 2005).

Statistics

Statistical analyses were performed using GraphPad Prism (GraphPad Software 9.0.0, La Jolla, CA, USA). Outliers were identified and removed using the ROUT method (Q = 1 %). Data are presented as box-and-whisker plots. Group comparisons were conducted using the Mann–Whitney U test. $P<0.05$ was considered statistically significant. Post-hoc power analyses were conducted for each experiment, and the exact sample sizes for all analyses are provided in Supplementary information (Supplementary Table 2).

RESULTS

Long-term WD feeding led to significant weight gain and liver damage compared to SD controls. Bone structure, particularly trabecular microarchitecture, worsened, but three-point bending tests suggested no significant impairment in cortical bone mechanical properties. Molecular studies revealed increased osteoclast activity without notable changes in osteoblast markers. Histological analyses further demonstrated an expansion of bone marrow adipose tissue and an increased abundance of CD163-positive macrophage lineage cells in WD-fed mice. Liver analysis showed downregulation of vitamin D 25-hydroxylases and related pathways, which was accompanied by reduced circulating 25-hydroxyvitamin D levels. Additionally, bone tissue demonstrated reduced VDR protein levels.

EXCLI Journal 2026;25:290-309 – ISSN 1611-2156
Received: November 03, 2025, accepted: January 14, 2026, published: January 23, 2026

Long-term WD feeding induces obesity and hepatic injury

Prolonged WD feeding led to a significant increase in body weight starting from week 3 compared to the SD control group (Figure 2A). At week 48, WD-fed mice exhibited a significantly elevated liver-to-body weight ratio (Figure 2B), accompanied by a trend toward increased random blood glucose levels (Figure 2C), suggestive of hepatic dysfunction. Biochemical assays confirmed hepatic injury, as evidenced by markedly increased plasma levels of alanine aminotransferase (ALT), aspartate aminotransferase (AST), and alkaline phosphatase (ALP) in WD-fed mice (Figure 2D–F).

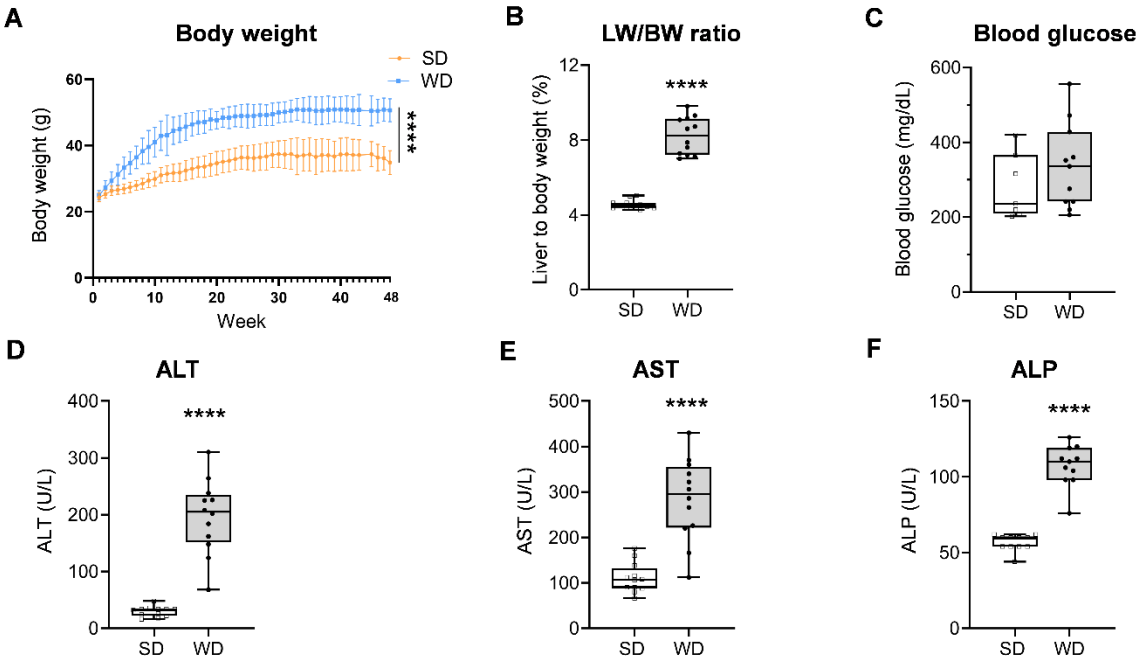

Figure 2: WD induces obesity and hepatic injury. (**A**) Changes in body weight of mice over the experimental period. (**B**) Liver-to-body weight ratio at week 48. (**C**) Random blood glucose levels were measured at week 48. (**D-F**) Plasma activities of alanine aminotransferase (ALT), aspartate aminotransferase (AST), and alkaline phosphatase (ALP) between groups at week 48. Data are presented as box-and-whisker plots. Statistical analysis was performed using the Mann–Whitney U test. *** $p < 0.001$, **** $p < 0.0001$ as compared to SD group. SD = standard diet, WD = Western diet

WD impairs trabecular microarchitecture and reduces bone mineral density

To evaluate the impact of obesity and hepatic injury on bone structure, we performed µCT on the distal femur. Representative µCT and 3D reconstructed images (Figure 3A-B) showed significantly damaged microarchitecture of the femur. Quantitative analysis revealed significant reductions in bone mineral density (BMD), tissue volume (TV), bone volume (BV), and the BV/TV ratio, along with a lower trabecular number and increased trabecular separation in the WD group (Figure 3C).

EXCLI Journal 2026;25:290-309 – ISSN 1611-2156
Received: November 03, 2025, accepted: January 14, 2026, published: January 23, 2026

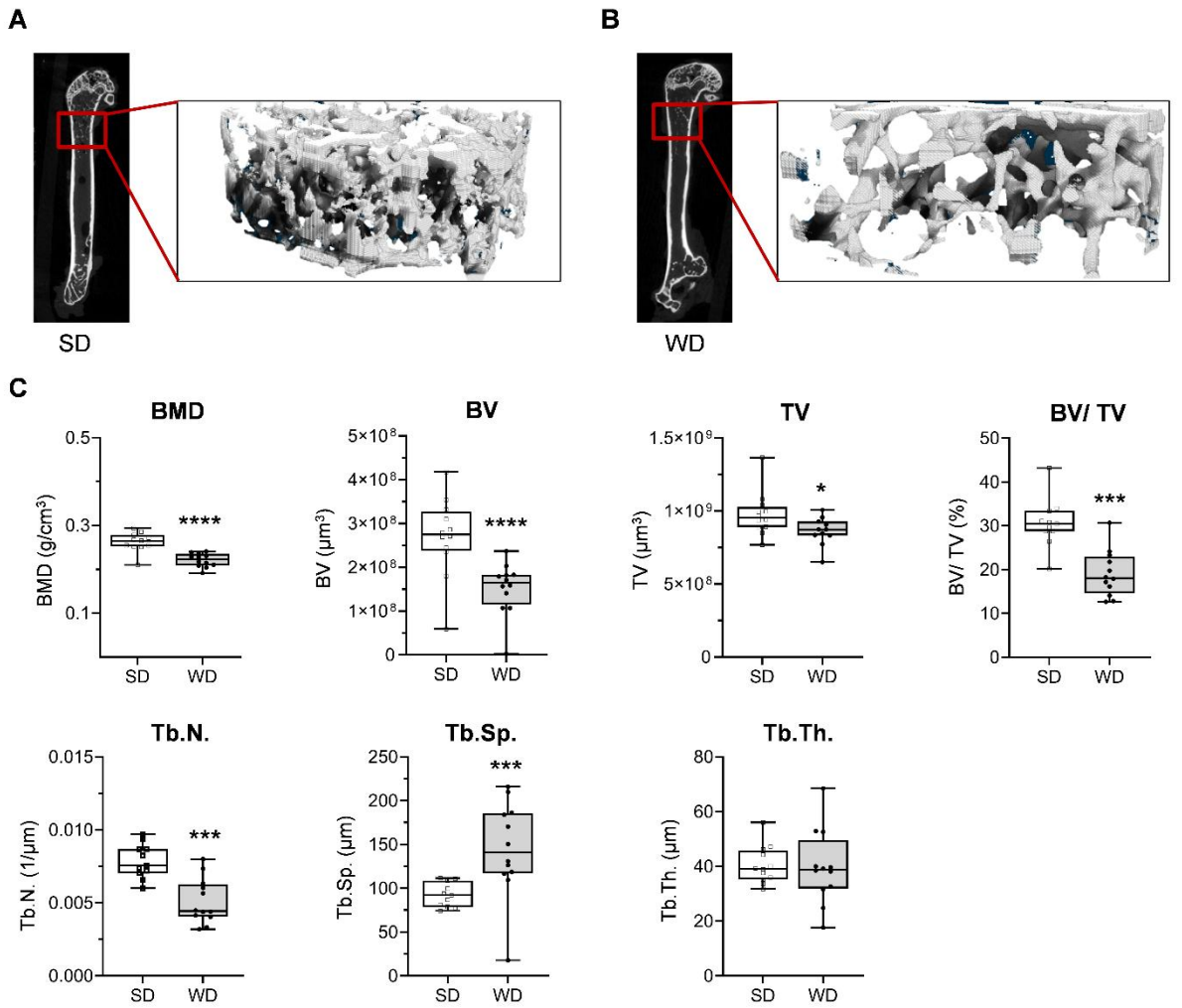

Figure 3: Obesity impairs trabecular bone microarchitecture in the distal femur. (**A-B**) Representative µCT and 3D reconstructed images of the distal femur from SD- and WD-fed mice. (**C**) Quantitative analysis of bone parameters, including bone mineral density, tissue volume, bone volume, bone volume to tissue volume ratio, trabecular number, trabecular separation, and trabecular thickness. All analyses were performed after 48 weeks of feeding. Data are presented as box-and-whisker plots. Statistical analysis was performed using the Mann–Whitney U test. * $p < 0.05$, ** $p < 0.01$, *** $p < 0.001$, **** $p < 0.0001$ as compared to SD group. SD = standard diet, WD = Western diet.

WD had no impact on bone mechanical properties

A three-point bending test was performed to further assess alterations in cortical bone mechanical properties (Figure 4). A trend towards increased bending stiffness in WD-fed mice was shown, but no statistical significance was reached (Figure 4A). Consistently, the yield load—defined as the force required to initiate permanent deformation—was comparable between groups (Figure 4B). Likewise, the ultimate load, representing the maximum force sustained before fracture, showed no significant intergroup variation (Figure 4C). In addition, the work-to-fracture, an indicator of bone toughness reflecting the total energy absorbed before fracture, also remained unchanged between the two groups (Figure 4D).

EXCLI Journal 2026;25:290-309 – ISSN 1611-2156
Received: November 03, 2025, accepted: January 14, 2026, published: January 23, 2026

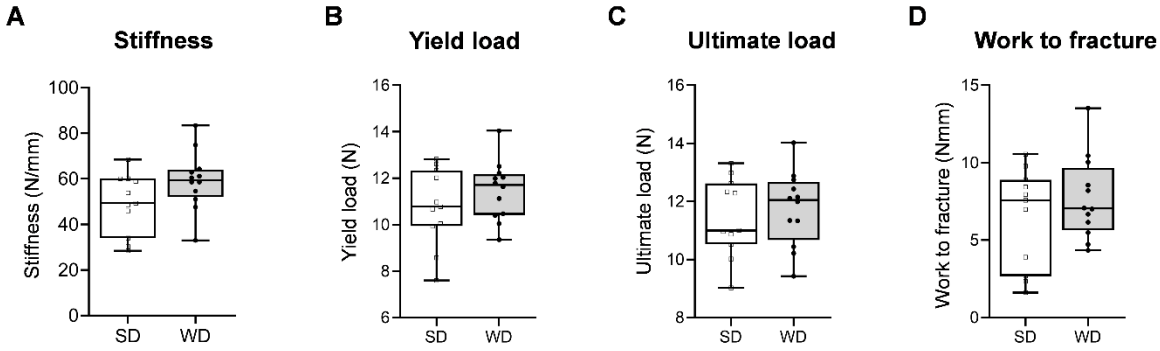

Figure 4: Effects of obesity on tibia mechanical properties assessed by three-point bending test. (**A**) Bending stiffness (N/mm), (**B**) yield load (N), (**C**) ultimate load (N), and (**D**) work to fracture (N·mm) were quantified to evaluate cortical bone strength and resistance to failure. The analyses were performed at week 48 after the onset of the diet feeding. Data are shown as box-and-whisker plots; Statistical analysis was performed using the Mann–Whitney U test. SD = standard diet, WD = Western diet

WD enhances osteoclastogenesis without affecting osteoblast markers

To explore cellular changes associated with bone loss, we analyzed the expression of bone remodeling-related markers in femoral tissue. Consistent with the trabecular bone parameters observed in WD-fed mice, RT-PCR analysis showed that the expression of *Csf1* (M-CSF) and *Tnfrsf11a* (RANK) was significantly increased in the WD group (Figure 5A-B). *Acp5* (TRAP) expression exhibited a modest increasing trend; however, this difference did not reach statistical significance (Figure 5C). In contrast, the expression levels of osteoblast-related genes remained comparable between SD- and WD-fed mice (Figure 5E-F).

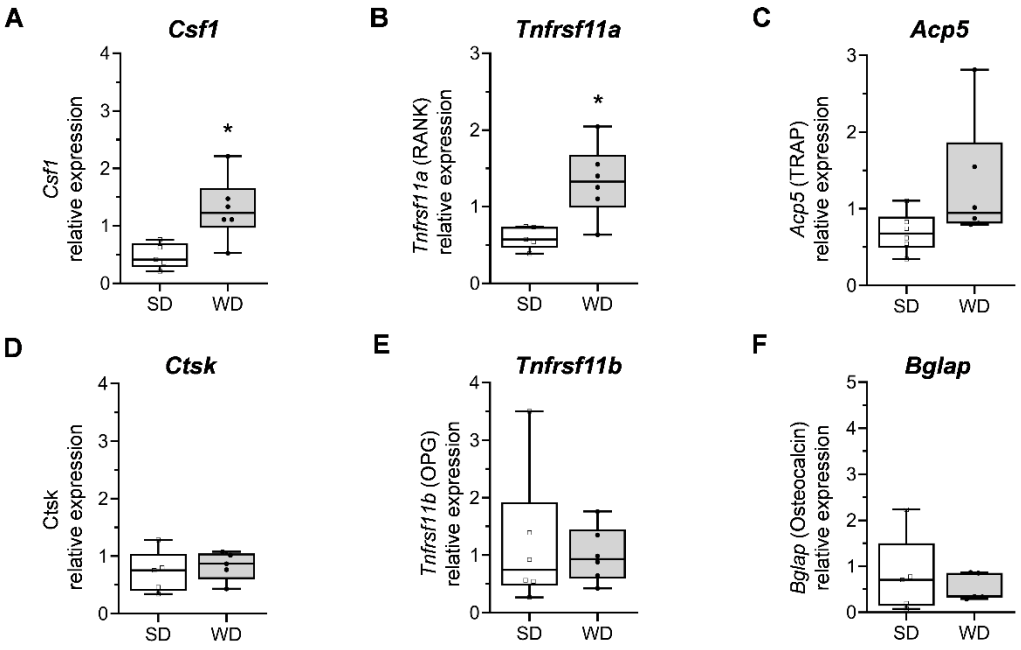

Figure 5: Expression of bone remodeling markers in femoral tissue of SD and WD mice. Differential expression of osteoclast and osteoblast marker genes between groups at Week 48. (**A**) Colony-stimulating factor 1 (*Csf1*), (**B**) Receptor activator of nuclear factor κB (*Tnfrsf11a*), (C) Tartrate-resistant acid phosphatase (*Acp5*), and (**D**) Cathepsin K (*Ctsk*). Expression levels of osteoblast-related genes are shown in (**E**) Osteoprotegerin (*Tnfrsf11b*) and (**F**) Osteocalcin (*Bglap)*. Data are shown as box-and-whisker plots; Statistical analysis was performed using the Mann–Whitney U test. * $p < 0.05$ as compared to SD group. SD = standard diet, WD = Western diet.

EXCLI Journal 2026;25:290-309 – ISSN 1611-2156
Received: November 03, 2025, accepted: January 14, 2026, published: January 23, 2026

WD alters the bone marrow microenvironment

Histological analysis revealed that WD feeding markedly altered the bone marrow microenvironment. Perilipin immunostaining demonstrated a clear increase in marrow adipocytes in WD-fed mice compared with SD controls, with adipocytes appearing more abundant and clustered in WD samples (Figure 6A). Quantitative analyses confirmed significant elevations in perilipin-positive adipocytes in the WD group (Figure 6B). CD163 immunohistochemistry also showed an increase in CD163-positive macrophages in WD-fed mice, indicating enhanced monocyte/macrophage lineage presence within the marrow (Figure 6C). Quantitative analyses confirmed significant elevations in CD163-positive macrophages in the WD group (Figure 6D).

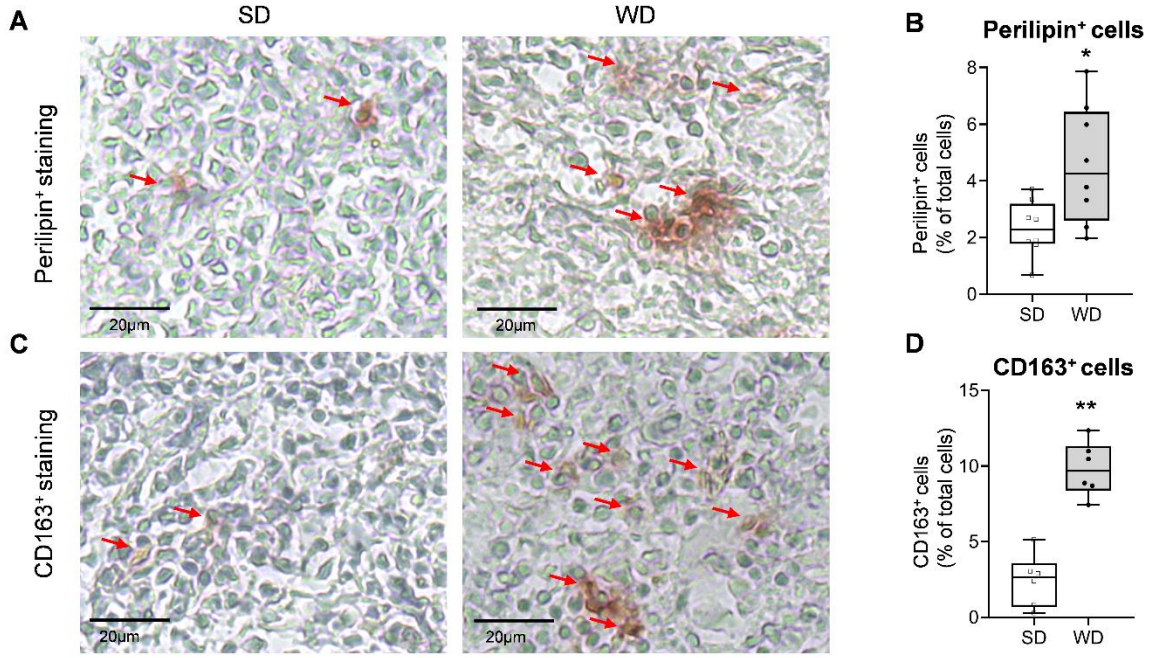

Figure 6: Histological assessment of bone composition. (**A**) Representative image of perilipin-positive adipocytes (arrowheads) from SD and WD mice at week 48. Scale bars: 20 µm. The average nuclear area was 14.67 µm² in SD mice and 14.22 µm² in WD mice. (**B**) Quantitative analysis of perilipin-positive adipocytes from the two groups. (**C**) Representative image of CD163-positive macrophage (arrowheads) from SD and WD mice at week 48. (**D**) Quantitative analysis of CD163-positive macrophages from the two groups. Scale bars: 20 µm. The average nuclear area was 14.43 µm² in SD mice and 14.50 µm² in WD mice. Data are shown as box-and-whisker plots. Statistical analysis was performed using the Mann–Whitney U test. * $p < 0.05$, ** $p < 0.01$ as compared to SD group. SD = standard diet, WD = Western diet.

Liver dysfunction impairs vitamin D biosynthesis, transport and absorption

Given that obesity alters the complex interplay between the liver and bone, we next investigated whether liver dysfunction in WD-fed mice contributes to the observed skeletal phenotype. RNA sequencing was performed on liver samples from both groups. Differential gene expression analysis was conducted using the DESeq2 package. A total of 864 differentially expressed genes (DEGs) (Supplementary information, Supplementary Table 3) were identified between the WD and SD groups.

To explore the potential biological functions of these DEGs between obese and control mice, Gene Ontology (GO) and Kyoto Encyclopedia of Genes and Genomes (KEGG) enrichment analyses were conducted. In the biological process (BP) category of GO analysis, the

EXCLI Journal 2026;25:290-309 – ISSN 1611-2156
Received: November 03, 2025, accepted: January 14, 2026, published: January 23, 2026

downregulated genes in obese mice were significantly enriched in lipid metabolic processes, cholesterol biosynthetic processes, and sterol biosynthetic processes (Figure 7A). Consistently, KEGG pathway analysis revealed significant enrichment in cholesterol and steroid hormone biosynthesis pathways (Figure 7B), suggesting suppressed hepatic lipid metabolism in obesity.

In contrast, the upregulated genes were primarily enriched in immune-related pathways, including immune system processes, chemokine signaling, and osteoclast differentiation (Supplementary information, Supplementary Figure 1A and 1B).

To test the hypothesis that the observed downregulation of cholesterol and steroid hormone biosynthesis genes may imply compromised hepatic vitamin D metabolism, GSEA with a defined vitamin D metabolism gene set (*Cyp2r1, Cyp27a1, Cyp24a1, Gc, Lrp2, Dhcr7, Rxra, Vdr, Cyp27b1*) was performed. GSEA results revealed that this gene set was significantly enriched at the top of the ranked gene list (NES = 1.43, FDR < 0.05), suggesting a coordinated downregulation of vitamin D metabolic genes in the WD group (Figure 7C).

Further hepatic transcriptome profiling identified significant downregulation of key vitamin D metabolic enzymes, including *Cyp2r1*, *Cyp27a1*, and *Gc (*vitamin D-binding protein, DBP*)*, in the WD group (Figure 7D). In addition, expression of *Cyp7a1*, the rate-limiting enzyme in the bile acid biosynthetic pathway in the liver, was also significantly decreased.

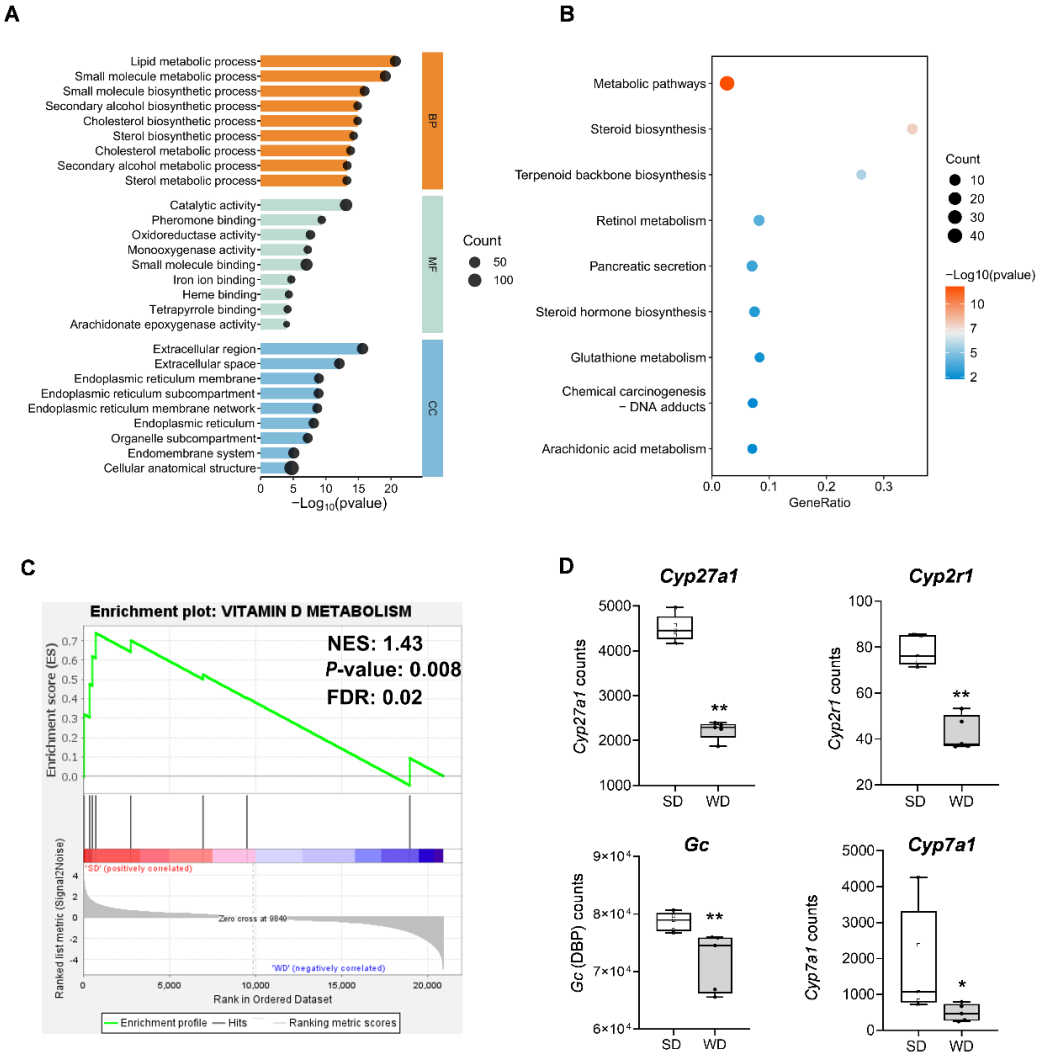

Figure 7: WD impairs hepatic cholesterol and vitamin D metabolism in obese mice. (**A**) GO enrichment analysis of differentially downregulated genes was performed based on three categories: biological process (BP), molecular function (MF), and cellular component (CC). (**B**) Pathway enrichment

analysis was performed using differentially downregulated genes based on the KEGG database. (**C**) GSEA was performed using a predefined vitamin D metabolism–related gene set. (**D**) Hepatic expression of key enzymes involved in vitamin D biosynthesis, transport and absorption, including *Cyp27a1*, *Cyp2r1*, *Gc* and *Cyp7a1*. Analysis was performed at week 48. Data are shown as box-and-whisker plots; Statistical analysis was performed using the Mann–Whitney U test. * $p < 0.05$, ** $p < 0.01$. SD = standard diet, WD = Western diet.

Impaired hepatic vitamin D metabolism disrupts systemic vitamin D availability and skeletal VDR signaling

To validate that hepatic metabolic dysfunction compromises vitamin D biosynthesis and transport, circulating 25(OH)D levels were quantified. As expected, plasma 25(OH)D concentrations were significantly decreased in the WD group compared with the SD controls (Figure 8A), consistent with the transcriptional suppression of hepatic vitamin D metabolic enzymes observed in WD-fed mice.

To further determine whether reduced systemic vitamin D availability affects skeletal vitamin D signaling, *Vdr* gene expression and protein levels were assessed. RT-PCR analysis revealed a significant upregulation of *Vdr* mRNA expression in the WD group compared to the SD group (Figure 8B). However, Western blot analysis demonstrated a pronounced reduction in VDR protein abundance in bone from obese mice (Figure 8C).

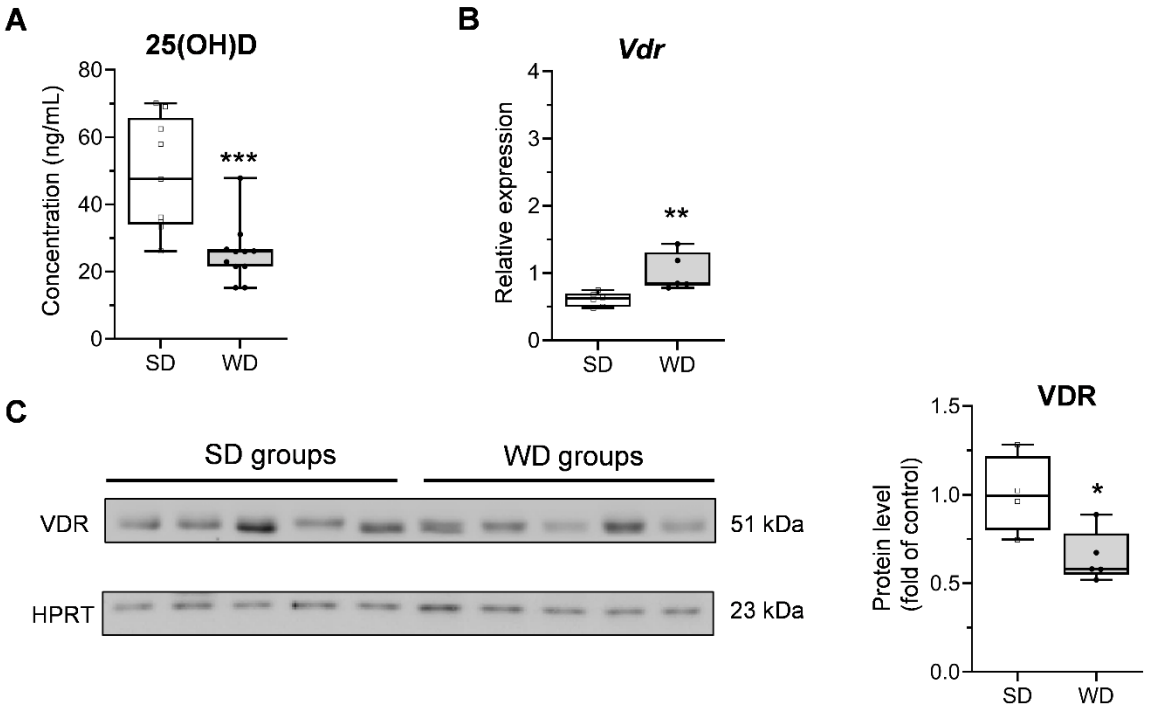

Figure 8: WD decreases the circulating 25(OH)D levels and suppresses vitamin D signaling in bones. (**A**) Plasma concentrations of circulating 25(OH)D. (**B**) Quantification of bone *Vdr* transcript levels normalized to *Actb.* (**C**) Representative Western blot images and quantification of VDR protein levels normalized to HPRT protein. Analysis was performed at week 48 after onset of the diet. Data are shown as box-and-whisker plots; Statistical analysis was performed using the Mann–Whitney U test. * $p < 0.05$, ** $p < 0.01$, *** $p < 0.001$. SD = standard diet, WD = Western diet

DISCUSSION

Obesity has emerged as a global health crisis and is paradoxically associated with an increased risk of bone fractures. Despite the higher mechanical loading typically expected to promote bone formation, clinical and experimental studies have consistently reported compromised bone quality in obese individuals, particularly in non-weight-bearing bones such as the upper limbs (Prieto-Alhambra et al., 2012; Dimitri, 2019). In this study, we utilized a long-term WD model to investigate the structural, biomechanical, and molecular alterations underlying skeletal fragility in obesity, with particular focus on the liver-vitamin D-bone axis.

The WD employed in this study contained elevated saturated fats (primarily from lard), cholesterol, refined carbohydrates (fructose and sucrose), and a high cholesterol content, alongside a moderately reduced choline level. While choline is essential for phosphatidylcholine synthesis and very-low-density lipoprotein export from hepatocytes (Sherriff et al., 2016), the magnitude of reduction in this model is modest. In contrast, the 2 % cholesterol content represents a substantial dietary intervention, specifically designed to overcome the low intestinal cholesterol absorption in rodents and induce hepatic lipid accumulation (Eng and Estall, 2021). This combination of dietary cholesterol and simple sugars is known to synergistically promote steatohepatitis, systemic inflammation, and metabolic dysfunction (Liang et al., 2018; Stephenson et al., 2018; Parisse et al., 2025).

This distinction between diet composition effects and obesity per se is crucial for interpreting our findings. The bone deterioration observed likely reflects the convergent influence of both dietary components (high fat, cholesterol, refined sugars) and obesity-related factors (adipokines, systemic inflammation, insulin resistance). Recent studies support this multi-factorial model, demonstrating that different high-fat diet compositions can produce distinct metabolic and phenotypic outcomes even when caloric content is controlled (Janoschek et al., 2023; Li et al., 2024).

Long-term WD feeding led to significant deterioration of trabecular bone microarchitecture with reduced trabecular number and volume, increased trabecular separation, and decreased BMD. These structural impairments are hallmark features of osteoporosis (Chen and Kubo, 2014). These μCT measurements reflect changes in the distal femur trabecular compartment, which is highly sensitive to metabolic disturbances. In contrast, three-point bending assessed cortical bone at the tibial diaphysis and showed no significant mechanical impairment. This divergence likely reflects the differing responsiveness of trabecular and cortical bone, as well as the potential protective influence of increased mechanical loading in obesity. Clinically, similar patterns are observed, with obesity often preserving cortical strength at weight-bearing sites despite compromised trabecular quality (Farr and Dimitri, 2017). These findings highlight that trabecular deficits emerge earlier, whereas cortical mechanical changes may be delayed or site dependent, emphasizing the need to evaluate both bone quantity and quality in obesity-related skeletal fragility.

At the cellular level, the increased expression of *Csf1* (M-CSF) and *Tnfrsf11a* (RANK) observed in femoral tissue of WD-fed mice suggests a shift toward a microenvironment that may favor osteoclast differentiation and activity. Although *Acp5* (TRAP) expression showed only a non-significant upward trend, the combined changes in osteoclast-associated markers are consistent with the observed reduction in trabecular bone parameters. Notably, the expression of osteoblast-related genes was not altered, indicating that trabecular bone loss under long-term WD feeding may be primarily associated with changes in osteoclast-related pathways rather than impaired osteoblast gene expression. This imbalance was accompanied by significant expansion of bone marrow adipocytes, as evidenced by increased perilipin-positive adipocytes. The expansion of bone marrow adipose tissue (BMAT) represents more than simple space competition with osteoblasts. Bone marrow adipocytes actively suppress osteoblastogenesis

through paracrine mechanisms, including NF-κB-mediated inhibition of BMP signaling (Abdallah, 2017). Additionally, BMAT serves as a source of inflammatory mediators that further promote osteoclastic bone resorption (Muruganandan et al., 2020). The elevated CD163 staining observed in WD-fed mice supports the notion of enhanced osteoclastogenic potential, as $CD163^+$ cells represent monocyte–macrophage lineage populations that include osteoclast precursors (Gomez-Brouchet et al., 2021; Bai et al., 2024; Qian et al., 2024). An increase in this precursor pool is likely to promote osteoclast formation and accelerate bone resorption in WD mice. This heightened resorptive activity is also consistent with the reduced bone mineral content detected by μCT analysis.

Emerging evidence has highlighted the liver-bone axis in regulating skeletal homeostasis, with reports suggesting that up to 75 % of patients with chronic liver disease exhibit severe osteoporosis (Ehnert et al., 2019). The hepatic transcriptomic analysis indicated impaired hepatic vitamin D metabolic pathways in WD-fed mice. The hepatic suppression of vitamin D metabolism likely reflects the inflammatory and metabolic stress characteristic of MAFLD (Badmus et al., 2022, Portincasa et al., 2024). Chronic inflammation is known to impair CYP enzymes activity, thereby disrupting vitamin D biotransformation. The suppression of *Cyp2r1* and *Cyp27a1* represents a critical bottleneck in vitamin D bioactivation, potentially linking liver metabolic impairment to bone loss (Roizen et al., 2018). Several mechanisms have been proposed to explain the lower vitamin D levels observed in obese individuals, such as sequestration of vitamin D within expanded adipose tissue, reduced cutaneous synthesis due to decreased sunlight exposure, and impaired intestinal absorption (Bennour et al., 2022). However, direct evidence linking hepatic metabolic impairment to vitamin D deficiency has remained limited. Vitamin D 25‑hydroxylation has been considered a constitutive, unregulated step until recently (Roizen et al., 2019; Elkhwanky et al., 2020). Recent human studies following gastric bypass surgery have shown that weight loss increases *CYP2R1* expression in subcutaneous adipose tissue, suggesting recovery from obesity-induced suppression (Elkhwanky et al., 2020). Our results align with emerging evidence that hepatic vitamin D hydroxylases are dynamically regulated and may be key drivers of systemic vitamin D deficiency in metabolic disease (Zhu et al., 2021). Additionally, the expression of DBP, the main transporter of 25(OH)D in circulation, was significantly reduced in WD-fed mice. Since DBP is synthesized predominantly in the liver and is essential for vitamin D transport and bioavailability, its downregulation may exacerbate systemic vitamin D insufficiency (Safadi et al., 1999; Bouillon et al., 2019). Clinical studies have reported that low serum DBP levels correlate with reduced BMD (Martínez-Aguilar et al., 2019), further implicating impaired hepatic vitamin D metabolism in skeletal fragility.

Dietary vitamin D (contributing 10-20 % of total in humans and nearly 100 % in UVB-deprived laboratory mice) requires bile acid-mediated micellar solubilization for intestinal absorption (Deepika et al., 2025; Ghallab et al., 2025; Sahithi et al., 2025). Notably, Cyp27a1, is not only an ancillary vitamin D 25-hydroxylase but also a key enzyme initiating the alternative (acidic) pathway of bile acid synthesis (Chiang and Ferrell, 2020). High-fat diets and MAFLD are frequently associated with activation of the intestinal FXR-FGF15/19 axis, which markedly suppresses hepatic *Cyp7a1* and can also attenuate *Cyp27a1* expression (Wei et al., 2024). These changes disrupt bile acid synthesis and shift the bile acid pool toward a more hydrophobic profile, a compositional pattern known to reduce micellar solubilization capacity and thereby impair the intestinal absorption of vitamin D (Ferslew et al., 2015; Clifford et al., 2021). The marked downregulation of hepatic *Cyp27a1* and *Cyp7a1* observed in WD-fed mice therefore raises the possibility that impaired bile acid homeostasis may further exacerbate systemic vitamin D insufficiency by reducing the efficiency of dietary vitamin D uptake. Circulating 25(OH)D levels were significantly reduced in WD-fed mice, supporting the presence of vitamin D deficiency. Hepatic vitamin D deficiency lowers circulating 25(OH)D, thereby restricting

substrate availability for renal 1α-hydroxylase and ultimately diminishing systemic $1,25(OH)_2D$ production.

The paradoxical reduction in VDR protein despite elevated *Vdr* mRNA indicates an important post-transcriptional regulatory mechanism. VDR protein stability is highly dependent on ligand binding, as the receptor undergoes conformational changes upon binding $1,25(OH)_2D$, thereby protecting it from proteasomal degradation (Zenata and Vrzal, 2017). This deficiency promotes VDR degradation and may explain the reduced bone VDR protein observed.

VDR serves as the sole nuclear receptor for $1,25\ (OH)_2D$ (Pike et al., 2017). Upon ligand binding, VDR forms a heterodimer with retinoid X receptor alpha and regulates target gene transcription by binding to vitamin D response elements (van Driel and van Leeuwen, 2017). This pathway influences both osteoblast differentiation and osteoclast activity. Reduced VDR levels may therefore disrupt this balance and contribute to increased bone resorption. Increased expression of osteoclastogenic genes in WD mice is consistent with this and supports the finding that reduced VDR causes exacerbated bone loss with enhanced osteoclastic activity (Starczak et al., 2018, 2021; Gasperini et al., 2023).

Genetic and clinical evidence further support a causal role for impaired VDR signaling in the skeletal abnormalities observed in our WD-fed mice. Global VDR-knockout mice develop hypocalcemia, secondary hyperparathyroidism, disorganized growth plates, and severe osteomalacia, defects that are largely corrected by calcium/phosphate rescue diets and therefore demonstrate the essential role of VDR signaling in bone mineralization (Yoshizawa et al., 1997; Bikle, 2012). Consistent with these findings, VDR loss-of-function mutations in humans, termed Vitamin D-Dependent Rickets type-II (VDDR-II), present with severe rickets/osteomalacia and elevated $1,25(OH)_2D$ despite normal ligand supply, underscoring the indispensability of VDR protein for skeletal responsiveness to vitamin D (Malloy et al., 2014). Together, these genetic data support our conclusion that reduced VDR abundance can uncouple bone remodeling and contribute to skeletal fragility. In contrast, clinical trials using vitamin D analogs, such as calcitriol, alfacalcidol, and eldecalcitol, have demonstrated beneficial effects on BMD and fracture prevention (Tilyard et al., 1992; Matsumoto et al., 2011; Harada et al., 2012).

Several limitations should be acknowledged. First, our model does not allow for the separation of obesity and hepatic injury as independent variables. Future studies using targeted models (e.g., diet-induced obesity without liver injury, or liver-specific knockouts) are needed to dissect their individual contributions. Second, our study did not directly measure renal 1α-hydroxylase activity, despite the well-established role of the kidney in converting 25(OH)D to its active form (Deluca, 2014). It is therefore possible that compensatory upregulation of renal 1α-hydroxylation may occur in response to hepatic insufficiency. However, emerging evidence suggests that obesity and MAFLD are frequently associated with elevated PTH levels, which may reflect secondary hyperparathyroidism. Elevated PTH can stimulate renal 1α-hydroxylase, increasing $1,25(OH)_2D$ production, but it can also promote bone resorption and impair cortical bone integrity. Thus, the observed skeletal deterioration may result not only from reduced hepatic 25-hydroxylation but also from compensatory endocrine changes that disrupt bone remodeling.

In summary, our study demonstrates that long-term WD feeding induces obesity and hepatic dysfunction, which together impair vitamin D metabolism and bone homeostasis. The resulting downregulation of hepatic vitamin D activation and bone VDR protein levels promotes osteoclastogenesis and skeletal fragility. These findings highlight the importance of the liver–bone axis and suggest that restoring vitamin D signaling— either through dietary modification or pharmacological intervention —may represent a promising strategy to prevent bone loss in obesity and MAFLD.

Data availability

The data that support the findings of this study are available from the corresponding author upon reasonable request.

Acknowledgments

We thank Dr. Caren Linnemann for her essential help in isolating bone RNA and protein. The presented data are in part from Pengcheng Zhou's medical dissertation and Mohammad Majd Hammour's PhD thesis. Pengcheng Zhou is a China Scholarship Council fellow. We acknowledge support from the Open Access Publishing Fund of the University of Tübingen. The work was partially funded by institutional funds of the Siegfried Weller Institute, the DFG (HE2509/24-1; 517010379& 457840828), and the BMBF (031L0314D).

Author contribution

Pengcheng Zhou (PZ) and Mohammad Majd Hammour (MMH) contributed equally to this work and share first authorship.

Jan G. Hengstler (JGH), Andreas K. Nüssler (AKN), and Tanja C. Maisenbacher (TCM) jointly supervised the study.

Conceptualization and Study Design: JGH, AKN

Experimental Work: PZ, MMH, Romina H. Aspera-Werz (RAW), Sandra Hans (SH)

Data Analysis and Interpretation: PZ, MMH, TCM, Sabrina Ehnert (SE), Matthias W. Laschke (MWL), Ahmed Ghallab (AG)

RNA-Seq and Bioinformatics: Karolina Edlund (KE), MMH

Methodology Development: Maiju Myllys (MM), Zaynab Hobloss (ZH), Reham Hassan (ReH), Daniela González (DG), Rama Hendawi (RaH)

Manuscript Writing – Original Draft: PZ, MMH, AKN, TCM

Manuscript Review and Editing: RAW, SE, MWL, SH, AG, MM, ZH, ReH, DG, RaH, KE, JGH, AKN

Supervision and Project Administration: AG, JGH, AKN

Funding Acquisition: AKN, AG, JGH

All authors contributed to drafting the article or revising it critically for important intellectual content. All authors gave final approval of the version to be submitted.

Conflict of interest

The authors declare no conflict of interest.

REFERENCES

Abdallah BM. Marrow adipocytes inhibit the differentiation of mesenchymal stem cells into osteoblasts via suppressing BMP-signaling. J Biomed Sci. 2017;24 (1):11. doi: 10.1186/s12929-017-0321-4.

Akter R, Afrose A, Sharmin S, Rezwan R, Rahman MR, Neelotpol S. A comprehensive look into the association of vitamin D levels and vitamin D receptor gene polymorphism with obesity in children. Biomed Pharmacother. 2022;153:113285. doi: 10.1016/j.biopha.2022.113285.

Badmus OO, Hillhouse SA, Anderson CD, Hinds TD, Stec DE. Molecular mechanisms of metabolic associated fatty liver disease (MAFLD): functional analysis of lipid metabolism pathways. Clin Sci (Lond). 2022; 136(18):1347–66. doi: 10.1042/cs20220572.

Bai X, Wang Y, Ma X, Yang Y, Deng C, Sun M, et al. Periodontal ligament cells-derived exosomes promote osteoclast differentiation via modulating macrophage polarization. Scientific Reports. 2024;14(1):1465. doi: 10.1038/s41598-024-52073-9.

Bathina S, Armamento-Villareal R. The complex pathophysiology of bone fragility in obesity and type 2 diabetes mellitus: therapeutic targets to promote osteogenesis. Front Endocrinol (Lausanne). 2023;14: 1168687. doi: 10.3389/fendo.2023.1168687.

Bennour I, Haroun N, Sicard F, Mounien L, Landrier JF. Vitamin D and Obesity/Adiposity-A Brief Overview of Recent Studies. Nutrients. 2022;14(10):2049. doi: 10.3390/nu14102049.

Bikle DD. Vitamin D and bone. Curr Osteoporos Rep. 2012;10(2):151–9. doi: 10.1007/s11914-012-0098-z.

Bouillon R, Schuit F, Antonio L, Rastinejad F. Vitamin D Binding Protein: A Historic Overview. Front Endocrinol (Lausanne). 2019;10:910. doi: 10.3389/fendo.2019.00910.

Chen H, Kubo KY. Bone three-dimensional microstructural features of the common osteoporotic fracture sites. World J Orthop. 2014;5(4):486–95. doi: 10.5312/wjo.v5.i4.486.

Chiang JYL, Ferrell JM. Bile acid receptors FXR and TGR5 signaling in fatty liver diseases and therapy. Am J Physiol Gastrointest Liver Physiol. 2020;318(3): G554–g73. doi: 10.1152/ajpgi.00223.2019.

Clifford BL, Sedgeman LR, Williams KJ, Morand P, Cheng A, Jarrett KE, et al. FXR activation protects against NAFLD via bile-acid-dependent reductions in lipid absorption. Cell Metab. 2021;33(8):1671–84.e4. doi: 10.1016/j.cmet.2021.06.012.

Compston JE, Watts NB, Chapurlat R, Cooper C, Boonen S, Greenspan S, et al. Obesity is not protective against fracture in postmenopausal women: GLOW. Am J Med. 2011;124(11):1043–50. doi: 10.1016/j.amjmed.2011.06.013.

Deepika, Kumari A, Singh S, Ahmad MF, Chaki D, Poria V, et al. Vitamin D: recent advances, associated factors, and its role in combating non-communicable diseases. NPJ Sci Food. 2025;9(1):100. doi: 10.1038/s41538-025-00460-5.

Deluca HF. History of the discovery of vitamin D and its active metabolites. Bonekey Rep. 2014;3:479. doi: 10.1038/bonekey.2013.213.

Dimitri P. The Impact of Childhood Obesity on Skeletal Health and Development. J Obes Metab Syndr. 2019;28(1):4–17. doi: 10.7570/jomes.2019.28.1.4.

Ehnert S, Aspera-Werz RH, Ruoß M, Dooley S, Hengstler JG, Nadalin S, et al. Hepatic Osteodystrophy-Molecular Mechanisms Proposed to Favor Its Development. Int J Mol Sci. 2019;20(10):2555. doi: 10.3390/ijms20102555.

Elkhwanky MS, Kummu O, Piltonen TT, Laru J, Morin-Papunen L, Mutikainen M, et al. Obesity Represses CYP2R1, the Vitamin D 25-Hydroxylase, in the Liver and Extrahepatic Tissues. JBMR Plus. 2020;4(11): e10397. doi: 10.1002/jbm4.10397.

Eng JM, Estall JL. Diet-Induced Models of Non-Alcoholic Fatty Liver Disease: Food for Thought on Sugar, Fat, and Cholesterol. Cells. 2021;10(7):1805. doi: 10.3390/cells10071805.

Farr JN, Dimitri P. The Impact of Fat and Obesity on Bone Microarchitecture and Strength in Children. Calcif Tissue Int. 2017;100(5):500–13. doi: 10.1007/s00223-016-0218-3.

Ferslew BC, Xie G, Johnston CK, Su M, Stewart PW, Jia W, et al. Altered Bile Acid Metabolome in Patients with Nonalcoholic Steatohepatitis. Dig Dis Sci. 2015; 60(11):3318–28. doi: 10.1007/s10620-015-3776-8.

Gao H, Peng X, Li N, Gou L, Xu T, Wang Y, et al. Emerging role of liver-bone axis in osteoporosis. Journal of Orthopaedic Translation. 2024;48:217–31. doi: https://doi.org/10.1016/j.jot.2024.07.008.

Gasperini B, Visconti VV, Ciccacci C, Falvino A, Gasbarra E, Iundusi R, et al. Role of the Vitamin D Receptor (VDR) in the Pathogenesis of Osteoporosis: A Genetic, Epigenetic and Molecular Pilot Study. Genes (Basel). 2023;14(3):542. doi: 10.3390/genes14030542.

Ghallab A, Myllys M, Friebel A, Duda J, Edlund K, Halilbasic E, et al. Spatio-Temporal Multiscale Analysis of Western Diet-Fed Mice Reveals a Translationally Relevant Sequence of Events during NAFLD Progression. Cells. 2021;10(10):2516. doi: 10.3390/cells10102516.

Ghallab A, Mandorfer M, Stirnimann G, Geyer J, Lindström E, Luedde T, et al. Enteronephrohepatic Circulation of Bile Acids and Therapeutic Potential of Systemic Bile Acid Transporter Inhibitors. J Hepatol. 2025;83(5):1204-1217. doi: 10.1016/j.jhep.2025.05.009.

Gkastaris K, Goulis DG, Potoupnis M, Anastasilakis AD, Kapetanos G. Obesity, osteoporosis and bone metabolism. J Musculoskelet Neuronal Interact. 2020; 20(3):372–81.

Gomez-Brouchet A, Gilhodes J, Van Acker N, Brion R, Bouvier C, Assemat P, et al. Characterization of Macrophages and Osteoclasts in the Osteosarcoma Tumor Microenvironment at Diagnosis: New Perspective for Osteosarcoma Treatment? Cancers. 2021;13(3): 423. doi: 10.3390/cancers13030423.

Harada S, Mizoguchi T, Kobayashi Y, Nakamichi Y, Takeda S, Sakai S, et al. Daily administration of eldecalcitol (ED-71), an active vitamin D analog, increases bone mineral density by suppressing RANKL expression in mouse trabecular bone. J Bone Miner Res. 2012;27(2):461–73. doi: 10.1002/jbmr.555.

Jacquillet G, Unwin RJ. Physiological regulation of phosphate by vitamin D, parathyroid hormone (PTH) and phosphate (Pi). Pflügers Archiv - European Journal of Physiology. 2019;471(1):83–98. doi: 10.1007/s00424-018-2231-z.

Janoschek R, Handwerk M, Hucklenbruch-Rother E, Schmitz L, Bae-Gartz I, Kasper P, et al. Heterogeneous effects of individual high-fat diet compositions on phenotype, metabolic outcome, and hepatic proteome signature in BL/6 male mice. Nutr Metab (Lond). 2023; 20(1):8. doi: 10.1186/s12986-023-00729-0.

Kawai T, Autieri MV, Scalia R. Adipose tissue inflammation and metabolic dysfunction in obesity. Am J Physiol Cell Physiol. 2021;320(3):C375–c91. doi: 10.1152/ajpcell.00379.2020.

Kolberg L, Raudvere U, Kuzmin I, Adler P, Vilo J, Peterson H. g:Profiler-interoperable web service for functional enrichment analysis and gene identifier mapping (2023 update). Nucleic Acids Res. 2023;51(W1): W207–w12. doi: 10.1093/nar/gkad347.

Latic N, Erben RG. FGF23 and Vitamin D Metabolism. JBMR Plus. 2021;5(12):e10558. doi: 10.1002/jbm4.10558.

Li YY, Madduri SS, Rezeli ET, Santos C, Freeman Iii H, Peng J, et al. Macronutrient-differential dietary pattern impacts on body weight, hepatic inflammation, and metabolism. Front Nutr. 2024;11:1356038. doi: 10.3389/fnut.2024.1356038.

Liang JQ, Teoh N, Xu L, Pok S, Li X, Chu ESH, et al. Dietary cholesterol promotes steatohepatitis related hepatocellular carcinoma through dysregulated metabolism and calcium signaling. Nat Commun. 2018;9(1): 4490. doi: 10.1038/s41467-018-06931-6.

Malloy PJ, Tasic V, Taha D, Tütüncüler F, Ying GS, Yin LK, et al. Vitamin D receptor mutations in patients with hereditary 1,25-dihydroxyvitamin D-resistant rickets. Mol Genet Metab. 2014;111(1):33–40. doi: 10.1016/j.ymgme.2013.10.014.

Martínez-Aguilar MM, Aparicio-Bautista DI, Ramírez-Salazar EG, Reyes-Grajeda JP, De la Cruz-Montoya AH, Antuna-Puente B, et al. Serum Proteomic Analysis Reveals Vitamin D-Binding Protein (VDBP) as a Potential Biomarker for Low Bone Mineral Density in Mexican Postmenopausal Women. Nutrients. 2019;11(12):2853. doi: 10.3390/nu11122853.

Matsumoto T, Ito M, Hayashi Y, Hirota T, Tanigawara Y, Sone T, et al. A new active vitamin D3 analog, eldecalcitol, prevents the risk of osteoporotic fractures--a randomized, active comparator, double-blind study. Bone. 2011;49(4):605–12. doi: 10.1016/j.bone.2011.07.011.

Muruganandan S, Ionescu AM, Sinal CJ. At the Crossroads of the Adipocyte and Osteoclast Differentiation Programs: Future Therapeutic Perspectives. Int J Mol Sci. 2020;21(7):2277. doi: 10.3390/ijms21072277.

Parisse S, Coltorti E, Mischitelli M, Ferri F, Ginanni Corradini S. New Insights into the Interplay Between Simple Sugars and Liver Diseases. Curr Issues Mol Biol. 2025;47(6):390. doi: 10.3390/cimb47060390.

Pike JW, Meyer MB, Lee SM, Onal M, Benkusky NA. The vitamin D receptor: contemporary genomic approaches reveal new basic and translational insights. J Clin Invest. 2017;127(4):1146–54. doi: 10.1172/jci88887.

Portincasa P, Khalil M, Mahdi L, Perniola V, Idone V, Graziani A, et al. Metabolic Dysfunction-Associated Steatotic Liver Disease: From Pathogenesis to Current Therapeutic Options. Int J Mol Sci. 2024;25(11):5640. doi: 10.3390/ijms25115640.

Prieto-Alhambra D, Premaor MO, Fina Avilés F, Hermosilla E, Martinez-Laguna D, Carbonell-Abella C, et al. The association between fracture and obesity is site-dependent: a population-based study in postmenopausal women. J Bone Miner Res. 2012;27(2):294–300. doi: 10.1002/jbmr.1466.

Qian J-k, Ma Y, Huang X, Li X-r, Xu Y-f, Liu Z-y, et al. The CD163/TWEAK/Fn14 axis: A potential therapeutic target for alleviating inflammatory bone loss. Journal of Orthopaedic Translation. 2024;49:82–95. doi: https://doi.org/10.1016/j.jot.2024.09.002.

Roizen JD, Casella A, Lai M, Long C, Tara Z, Caplan I, et al. Decreased Serum 25-Hydroxyvitamin D in Aging Male Mice Is Associated With Reduced Hepatic Cyp2r1 Abundance. Endocrinology. 2018;159(8): 3083–9. doi: 10.1210/en.2017-03028.

Roizen JD, Long C, Casella A, O'Lear L, Caplan I, Lai M, et al. Obesity Decreases Hepatic 25-Hydroxylase Activity Causing Low Serum 25-Hydroxyvitamin D. J Bone Miner Res. 2019;34(6):1068–73. doi: 10.1002/jbmr.3686.

Safadi FF, Thornton P, Magiera H, Hollis BW, Gentile M, Haddad JG, et al. Osteopathy and resistance to vitamin D toxicity in mice null for vitamin D binding protein. J Clin Invest. 1999;103(2):239–51. doi: 10.1172/jci5244.

Sahithi D, Nagarakanti S, Prudhvi SS, Gunupati S, Biradavolu S, Chiruvella B, et al. Vitamin D Levels and Their Association With Periodontitis in Women With Polycystic Ovary Syndrome: A Cross-sectional Study. Cureus. 2025;17(4):e82268. doi: 10.7759/cureus.82268.

Serdar MA, Arslan FD, Saral NY, Yücel D. Correlation between serum 1,25-dihydroxyvitamin D and 25-hydroxyvitamin D in response to analytical procedures; a systematic review and meta-analysis. Turkish Journal of Biochemistry. 2024;49(3):306–24. doi: doi:10.1515/tjb-2023-0258.

Sherriff JL, O'Sullivan TA, Properzi C, Oddo JL, Adams LA. Choline, Its Potential Role in Nonalcoholic Fatty Liver Disease, and the Case for Human and Bacterial Genes. Adv Nutr. 2016;7(1):5–13. doi: 10.3945/an.114.007955.

Starczak Y, Reinke DC, Barratt KR, Ryan JW, Russell PK, Clarke MV, et al. Absence of vitamin D receptor in mature osteoclasts results in altered osteoclastic activity and bone loss. J Steroid Biochem Mol Biol. 2018;177:77–82. doi: 10.1016/j.jsbmb.2017.10.022.

Starczak Y, Reinke DC, Barratt KR, Russell PK, Clarke MV, Davey RA, et al. Vitamin D receptor expression in mature osteoclasts reduces bone loss due to low dietary calcium intake in male mice. J Steroid Biochem Mol Biol. 2021;210:105857. doi: 10.1016/j.jsbmb.2021.105857.

Stephenson K, Kennedy L, Hargrove L, Demieville J, Thomson J, Alpini G, et al. Updates on Dietary Models of Nonalcoholic Fatty Liver Disease: Current Studies and Insights. Gene Expr. 2018;18(1):5–17. doi: 10.3727/105221617x15093707969658.

Subramanian A, Tamayo P, Mootha VK, Mukherjee S, Ebert BL, Gillette MA, et al. Gene set enrichment analysis: a knowledge-based approach for interpreting genome-wide expression profiles. Proc Natl Acad Sci U S A. 2005;102(43):15545–50. doi: 10.1073/pnas.0506580102.

Tilyard MW, Spears GF, Thomson J, Dovey S. Treatment of postmenopausal osteoporosis with calcitriol or calcium. N Engl J Med. 1992;326(6):357–62. doi: 10.1056/nejm199202063260601.

Turer CB, Lin H, Flores G. Prevalence of vitamin D deficiency among overweight and obese US children. Pediatrics. 2013;131(1):e152–61. doi: 10.1542/peds.2012-1711.

van Driel M, van Leeuwen J. Vitamin D endocrinology of bone mineralization. Mol Cell Endocrinol. 2017; 453:46–51. doi: 10.1016/j.mce.2017.06.008.

Via M. The malnutrition of obesity: micronutrient deficiencies that promote diabetes. ISRN Endocrinol. 2012;2012:103472. doi: 10.5402/2012/103472.

Wei M, Tu W, Huang G. Regulating bile acids signaling for NAFLD: molecular insights and novel therapeutic interventions. Front Microbiol. 2024;15: 1341938. doi: 10.3389/fmicb.2024.1341938.

Wintermeyer E, Ihle C, Ehnert S, Stöckle U, Ochs G, de Zwart P, et al. Crucial Role of Vitamin D in the Musculoskeletal System. Nutrients. 2016;8(6):319. doi: 10.3390/nu8060319.

Yao P, Bennett D, Mafham M, Lin X, Chen Z, Armitage J, et al. Vitamin D and Calcium for the Prevention of Fracture: A Systematic Review and Meta-analysis. JAMA Netw Open. 2019;2(12):e1917789. doi: 10.1001/jamanetworkopen.2019.17789.

Yoshizawa T, Handa Y, Uematsu Y, Takeda S, Sekine K, Yoshihara Y, et al. Mice lacking the vitamin D receptor exhibit impaired bone formation, uterine hypoplasia and growth retardation after weaning. Nat Genet. 1997;16(4):391–6. doi: 10.1038/ng0897-391.

Zenata O, Vrzal R. Fine tuning of vitamin D receptor (VDR) activity by post-transcriptional and post-translational modifications. Oncotarget. 2017;8(21):35390–402. doi: 10.18632/oncotarget.15697.

Zhao J, Lei H, Wang T, Xiong X. Liver-bone crosstalk in non-alcoholic fatty liver disease: Clinical implications and underlying pathophysiology. Frontiers in Endocrinology. 2023;14:1161402. doi: 10.3389/fendo.2023.1161402.

Zhu T, Zhao J, Zhuo S, Hu Z, Ouyang S, Wunier, et al. High Fat Diet and High Cholesterol Diet Reduce Hepatic Vitamin D-25-Hydroxylase Expression and Serum 25-Hydroxyvitamin D(3) Level through Elevating Circulating Cholesterol, Glucose, and Insulin Levels. Mol Nutr Food Res. 2021;65(21):e2100220. doi: 10.1002/mnfr.202100220.